Romanian Reports in Physics **76**, 505 (2024)

TUNABLE EMISSION COLOR OF NOVEL Y_3NbO_7:xDy^{3+} PHOSPHOR

Lj. ĐAČANIN FAR, A. ĆIRIĆ, J. PERIŠA, V. ĐORĐEVIĆ, Z. RISTIĆ, B. MILIĆEVIĆ, M. D. DRAMIĆANIN

Centre of Excellence for Photoconversion, Vinča Institute of Nuclear Sciences-National Institute of the Republic of Serbia, University of Belgrade, P.O. Box 522, 11001 Belgrade, Serbia
E-mails: *ljubica.far@vin.bg.ac.rs; aleksandarciric83@gmail.com; jburojevic@yahoo.com; vesipka@vin.bg.ac.rs; zoran.s.ristic@gmail.com; bojana.milicevic85@gmail.com; dramican@vinca.rs*

Received October 24, 2023

Abstract. Powders of Y_3NbO_7:xDy^{3+} (x = 0.5, 1, 1.5, 3 and 5 mol%) were produced through a solid-state process. X-ray diffraction investigations confirm the fluorite-type structure (space group $F_{m\bar{3}m}$) of powders with crystallite size in the range of 19–60 nm. Both the photoluminescence excitation and emission spectra revealed the presence of defects within the material. With different excitation wavelengths, the emission spectra exhibited distinct emission patterns. At each excitation wavelength, the emission was quenched at Dy^{3+} concentration higher than 1 mol%. The decay time measurements of the highest intensity emission revealed a progressive decrease from 0.472 milliseconds for x = 0.5 mol% to 0.246 milliseconds for x = 5 mol%. The CIE chromaticity coordinates investigation revealed that the emission color may be altered by varying the excitation wavelength, ranging from blue (excitation at 333 nm) and near-white (excitation at 353 nm and 390 nm) to orange (excitation at 457 nm). The chromaticity of emission under 353 nm and 390 nm excitation validated the material's suitability as an almost-white phosphor.

Key words: Yttrium niobate; lanthanide luminescence; Dy^{3+}; white LEDs.

DOI: https://doi.org/10.59277/RomRepPhys.2024.76.505

1. INTRODUCTION

Light-emitting materials, particularly phosphors, play a crucial role in our daily lives, and it is difficult to envisage technological advancement without them. In this regard, current research into light-emitting materials has two goals: discovering new materials and improving the capabilities of existing ones. Many mixed oxides of the Re_2O_3–M_2O_5 varied family of compounds (Re = Y, La, Lu; M = V, Nb, Ta, P) have been extensively studied due to the exceptional qualities they possess [1–5].

As yttrium niobates, the Y_2O_3–Nb_2O_5 combination exists in two forms: $YNbO_4$ and Y_3NbO_7. $YNbO_4$, a fergusonite-structured yttrium-niobate, proved to be an excellent host material for doping with a range of lanthanide ions [6–9]. Previous

research on $YNbO_4$ [10–12] demonstrated its high doping potential and strong temperature sensing characteristics. Fluorite's niobate analog, Y_3NbO_7, has been studied as a host for photoluminescent ions to a limited extent [13–17]. Our recent publication [18] was focused on the concentration quenching of Y_3NbO_7:Eu^{3+} emission and associated Judd-Ofelt parameterization.

White light emitting diodes (WLEDs) with stable and intense output are currently in high demand in display and lighting technology. Commercial WLEDs are comprised of a blue InGaN chip and a yellow-emitting YAG:Ce^{3+} phosphor, however, the absence of a red component results in disadvantages like a high associated color temperature and a low color rendering index. Possible solutions include integrating blue chips with red and green emitting phosphors, or merging red, blue, and green emitting phosphors onto near-UV chips [19, 20]. Using Dy^{3+}-doped phosphors [21] is a second approach that is simpler and less expensive. Dy^{3+} ions are exceptional in that they can produce emissions in the blue and yellow regions, and in some hosts, the red region of the spectrum [21]. Since the red emission of Dy^{3+}, if detected at all, is often of low intensity, the rendering index and color quality of the resulting white light are low. Nevertheless, near-white light emission can be achieved by modifying the yellow-to-blue intensity ratio value [21]. So, the focus of our research was on incorporating Dy^{3+} ions into the Y_3NbO_7 matrix and analyzing the resulting emission color, which may match the specifications for white LEDs.

Powders of $Y_{3-x}Dy_xNbO_7$ (x = 0.5, 1, 1.5, 3, 5 mol%) were produced for the first time utilizing a solid-state reaction method. We tested their emission under various wavelengths of excitation, obtaining tunable emission colors ranging from blue through white to orange. Additionally, the optimal concentration of Dy^{3+} ions was identified. Based on the CIE chromaticity study, we examined the quality of emission colors and the viability of employing these samples as phosphor-converted white LEDs.

2. EXPERIMENTAL

The powder samples of Y_3NbO_7 with different Dy^{3+} concentrations (0.5, 1, 1.5, 3, 5 mol%) were prepared using the starting precursors: Y_2O_3 (Alfa Aesar, 99.9%), Nb_2O_5 (Alfa Aesar, 99.5%), Dy_2O_3 (Alfa Aesar, 99.9%), while $Na_2SO_4 \cdot 10H_2O$ (Alfa Aesar, 99%) was added as flux, to facilitate the solid-state reaction between components. The precursors were mixed and homogenized in a vibrational ball mill (Anton Paar BM500). The whole procedure consisted of two cycles of milling and annealing, as it is described in detail in [18].

X-ray diffraction measurements obtained with a Rigaku SmartLab system operating with Cu Kα radiation at 30 mA and 40 kV were used to confirm the phase purity and crystallinity of the samples. Diffraction spectra were recorded in the 2θ range of 10°–90°, with 0.02° steps and 1°/min counting time. The corresponding results of the structural analysis were obtained using a built-in PDXL2 package software.

Scanning electron microscopy was used to observe powders' microstructure. The micrographs were taken using Mira3 Tescan field emission scanning electron microscope (FE-SEM), operating at 20 keV and with 20.00 kx magnification.

Photoluminescent properties of the samples were scrutinized using a Fluorolog-3 Model FL3-221 spectrofluorometer system (Horiba Jobin Yvon), equipped with a 450 W Xenon lamp and TBX detector. The excitation and emission spectra were recorded at room temperature at several different wavelengths. Excited-state lifetime measurements at room temperature were carried out using the FHR1000 Horiba Jobin Yvon spectrofluorometer system with an iCCD camera (Horiba Jobin Yvon 3771), by exciting samples with a 365-nm Ocean Optics fiber-coupled LED (L365A) and recording the emission at 575 nm.

3. RESULTS AND DISCUSSION

3.1. PHASE, STRUCTURAL, AND MICROSTRUCTURAL ANALYSIS

The Y_3NbO_7 compound crystallizes in a cubic fluorite-type structure, with a space group $F_{m\bar{3}m}$ [21–24]. This structure is schematically presented in Fig. 1, where the Y^{3+} and Nb^{5+} ions randomly occupy the cation 4a site in the 3:1 ratio. Oxygen ions are distributed at anion 8c sites, coordinating both Y^{3+} and Nb^{5+} ions octahedrally, while oxygen vacancies randomly occupy 1/8 of anion sites [22, 25]. However, the presence of O-vacancies can represent a drawback concerning photoluminescent properties, as they cause an intrinsic structural disorder that influences the spectroscopic properties of Eu^{3+} dopant ions within this host [14, 18]. Considering the size and electric charge [26], we can say that Dy^{3+} ions replace Y^{3+} ions within the fluorite Y_3NbO_7 structure, conserving their octahedral coordination with O^{2-} ions.

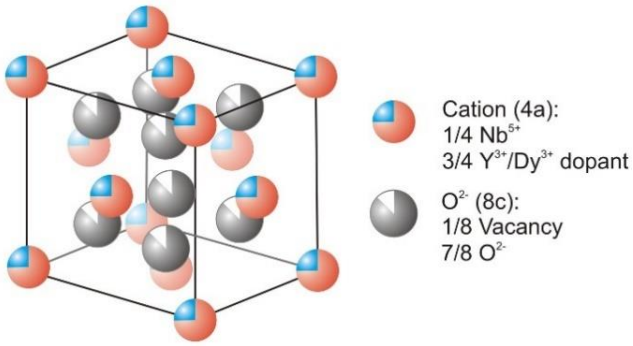

Fig. 1 – The structure of the Y_3NbO_7 compound.

Figure 2 displays the structural and microstructural characterization results. The X-ray diffraction patterns of the synthesized Y_3NbO_7: xDy^{3+} powders are shown

together with the standard data from the ICDD 01-074-6421 card. No diffraction peaks from impurity phases are observed, which suggests that this synthesis procedure enables the production of Dy^{3+}-doped single-phased powders of the same structure as the Y_3NbO_7 host. There is a slight trend in the peak shift towards lower 2θ values, proving that the dopant ions are effectively incorporated into the Y_3NbO_7 host. The representative SEM micrographs show the powders' microstructure characteristic for the solid-state synthesis procedure. The agglomerated particles of 1–2 micrometer sizes and irregular shapes can be distinguished from the smaller submicron chips that were formed during the milling process. As expected, the Dy^{3+} ions concentration does not influence the microstructure of the powders.

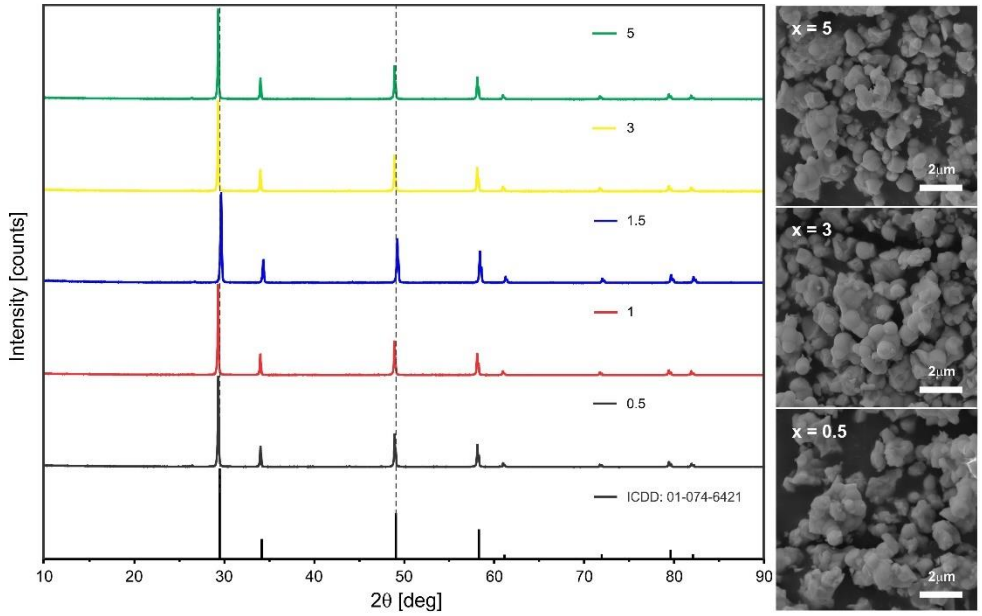

Fig. 2 – XRD spectra of Y_3NbO_7:$x$$Dy^{3+}$ samples (x = 0.5, 1, 1.5, 3, 5 mol%), the ICDD 01-074-6421 diffraction data and the representative SEM images of Y_3NbO_7:$x$$Dy^{3+}$ samples (x = 0.5, 3, 5 mol%).

The crystal lattice parameters given in Table 1 were determined using the built-in PDXL2 package software, and the initial parameters for the analysis were taken from [27]. The fitting parameters (profile factor [Rp], weighted profile factor [Rwp], and the expected weighted profile factor [Re], the goodness of fit [GOF]) are relatively small, indicating a reliable fitting outcome. The crystallite size varies from 19 nm to 60 nm and is more likely influenced by local inhomogeneities during the synthesis procedure than the Dy^{3+} ion content. The unit cell parameter exhibits only a slight variation with the increase in Dy^{3+} concentration. It is safe to say that the Dy^{3+} content is so small, it does not influence the structural parameters of the Y_3NbO_7 host.

Table 1

Structural details of the Y_3NbO_7 powder samples with different Dy^{3+} concentrations

x [mol% Dy^{3+}]	0.5	1	1.5	3	5
$a = b = c$ (Å)	5.25007(9)	5.25312(9)	5.24669(10)	5.25303(8)	5.25206(10)
Crystallite size (Å)	606(3)	427(6)	186(4)	424(7)	345(4)
Strain (%)	0.49(10)	0.11(3)	0.31(7)	0.11(3)	0.14(3)
Rwp (%)	10.08	11.94	16.46	10.49	15.73
Rp (%)	8.19	8.99	10.04	8.24	10.90
Re (%)	2.85	2.83	3.10	2.79	2.71
GOF	3.5396	4.2235	5.3047	3.7534	5.8037

3.2. STEADY-STATE PHOTOLUMINESCENCE SPECTROSCOPY

The photoluminescence excitation spectra of Y_3NbO_7:xDy^{3+} powders, recorded under different emission wavelengths are shown in Fig. 3. When the emission is fixed at 579 nm ($^4F_{9/2} \rightarrow {}^6H_{13/2}$ transition of Dy^{3+}), the excitation spectra in Fig. 3a displays narrow peaks that occur due to typical $4f \rightarrow 4f$ electronic transitions of Dy^{3+} ions. The excitation transitions from the $^6H_{15/2}$ ground level to the following upper energy levels appear at: 326 nm ($\rightarrow {}^4M_{17/2}$) 353 nm ($\rightarrow {}^6P_{7/2}+{}^4M_{15/2}$), 365 nm ($\rightarrow {}^6P_{5/2}+{}^6P_{3/2}$), 387 + 392 nm ($\rightarrow {}^4K_{17/2} + {}^4F_{7/2}+{}^4I_{13/2}$), 426 nm ($\rightarrow {}^4G_{11/2}$), 449+456 nm ($\rightarrow {}^4I_{15/2}$), 473 nm ($\rightarrow {}^4F_{9/2}$) [28–30]. The sample with 1 mol% exhibits the strongest excitation intensity. By monitoring the emission at 394 nm, we recorded the wide excitation band, peaking at about 329 nm (Fig. 3b) which originates from the excitation of the matrix's defects. As proven before, the presence of oxygen vacancies within the fluorite structure can cause an intrinsic structural disorder that affects photoluminescent properties [14, 18].

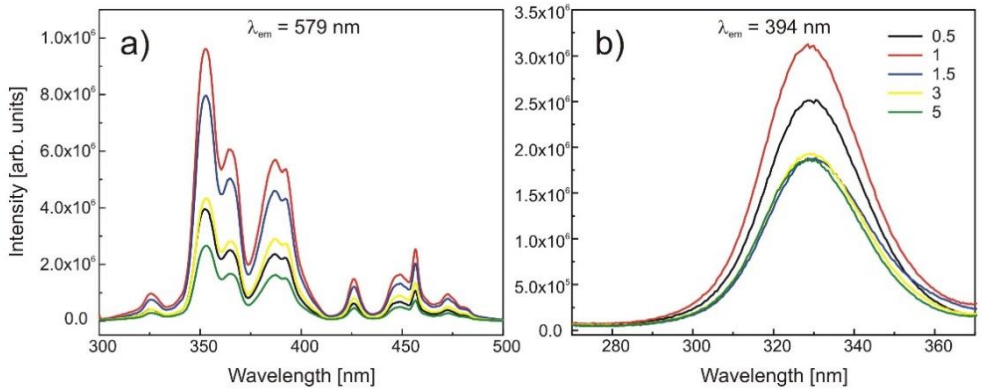

Fig. 3 – Excitation spectra of Y_3NbO_7:xDy^{3+} samples (x = 0.5, 1, 1.5, 3, 5 mol%), recorded under: a) λ_{em} = 579 nm; b) λ_{em} = 394 nm emission wavelengths.

The emission spectra of $Y_3NbO_7:Dy^{3+}$ under various excitations and Dy^{3+} concentrations are shown in Fig. 4. When the samples are excited by 353 and 390 nm (Fig. 4a and Fig. 4b, respectively), they exhibit standard emission peaks of Dy^{3+} ion, located around 480 nm ($^4F_{9/2} \rightarrow {}^6H_{11/2}$ transition), 580 nm ($^4F_{9/2} \rightarrow {}^6H_{13/2}$ transition) and 670 nm ($^4F_{9/2} \rightarrow {}^6H_{15/2}$ transition) [21]. The $^4F_{9/2} \rightarrow {}^6H_{13/2}$ transition is the most intense, being subjected to the hypersensitivity selection rule $\Delta J = \pm 2$ [31]. This means there is a lack of inversion symmetry of the crystallographic sites where the dopant Dy^{3+} ions are situated [32]. Since XRD analysis proved that all the synthesized powders have crystallized in the $F_{m\bar{3}m}$ space group and that substituting Y^{3+} with Dy^{3+} is not affecting the existing symmetry of the host, the origin of the disorder can be explained by the presence of oxygen vacancies [15]. In this study, the oxygen vacancies are presumably introduced during the milling in the synthesis process. The red emission transition around 670 nm is also recorded and is of the lowest intensity.

The emission obtained under the 333 nm excitation (Fig. 4c) reveals a strong band in the blue region, peaking at 400 nm, that surpasses the emission peaks of the Dy^{3+} ion. It is the first time that a defect type of emission is reported in Y_3NbO_7-based phosphors and it resembles the blue emission of the undoped $YNbO_4$ when excited with UV or X-rays, which occurs due to charge transfer from the oxygen to niobium within the NbO_4^{3-} tetrahedron groups inside the lattice [33–35]. In the fluorite Y_3NbO_7 structure, both Y^{3+} and Nb^{5+} ions are octahedrally coordinated to oxygen, but the presence of oxygen vacancies can introduce perturbation into this arrangement. Thus, we can safely assume the strongest emission band in Fig. 4c originates from the $O^{2-} – Nb^{5+}$ charge transfer within the defect tetrahedrons inside the matrix.

Upon excitation with 457 nm, the synthesized $Y_3NbO_7:xDy^{3+}$ powders exhibit a two-band emission from Dy^{3+} transitions, while the yellow one around 578 nm convincingly dominates. A low intensity infrared band around 760 nm is visible as well. It is displayed in a magnified image and originates from the $^4F_{9/2} \rightarrow {}^6H_{9/2}$ transition.

From the insets in Fig. 4, where the integrated emission intensity is depicted as the function of Dy^{3+} concentration, it is obvious that the concentration quenching of emission occurs after 1 mol% of Dy^{3+}. As there is no available data on Dy^{3+}-doped Y_3NbO_7, we compared this result to the dysprosium emission in the $YNbO_4$ matrix [36]. In this study, the critical concentration is lower than in [36], which is to be expected since the same applies to Eu^{3+} ions in these niobate matrixes [18]. The concentration dependence has got almost identical profiles for all different excitation wavelengths, except for the dominantly defect-originated emission at $\lambda_{ex} = 333$ nm (Fig. 4c). The main contribution to this emission does not come from the Dy^{3+} ion itself, so we cannot discuss the influence of it on the overall integrated emission intensity.

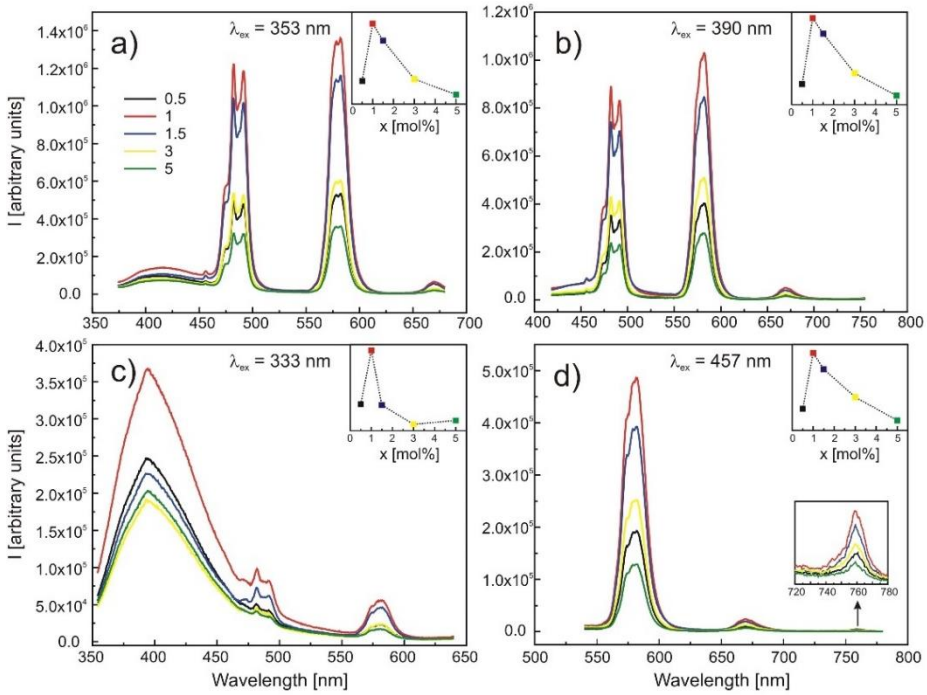

Fig. 4 – Emission spectra of Y_3NbO_7:xDy^{3+} samples (x = 0.5, 1, 1.5, 3, 5 mol%), recorded under: a) λ_{ex} = 353 nm; b) λ_{ex} = 390 nm; c) λ_{ex} = 333 nm and d) λ_{ex} = 457 nm, excitation wavelengths. Insets display the concentration dependence of integrated emission intensities.

3.3. TIME-RESOLVED PHOTOLUMINESCENCE SPECTROSCOPY

A lifetime of the photoluminescent emission from the excited state (τ) is defined by the following equation:

$$\tau = \left(\sum A_R + A_{NR}\right)^{-1} \tag{1}$$

where A_R and A_{NR} are radiative and non-radiative transition rates, respectively.

Figure 5a shows curves of the emission decay upon the 365 nm excitation for samples with different Dy^{3+} concentrations. These data were fitted using the single-exponential model:

$$I(t) = I(0) \cdot \exp\left(-\frac{t}{\tau}\right) \tag{2}$$

and the lifetime values are obtained from the fits (Fig. 5b). The lifetime value is the highest for the 0.5 mol%-doped sample (τ = 0.472 ms), after which it declines with

the increase of Dy^{3+} concentration down to τ = 0.246 ms. The distribution of lifetimes does not coincide with the concentration quenching of emission (Fig. 4), and the main process responsible for the emission lifetimes decrease is the cross-relaxation between Dy^{3+} ions [37]. The explanation for this is that the radiative transition rate is the same regardless of concentration, while A_{NR} monotonously increases with Dy^{3+} concentration because of the cross-relaxation mechanism, leading to lifetime values decrease. The calculated lifetime values can be compared to the recent decay lifetime data of $Ba_2GdV_3O_{11}$:0.04Dy^{3+} (0.47 ms) [38], $LiNbO_3$:0.02Dy^{3+} (0.215 ms) [39] and $KCa_2Nb_3O_{10}$:0.20Dy^{3+} (0.160 ms) [40], indicating the samples in this study are promising phosphors.

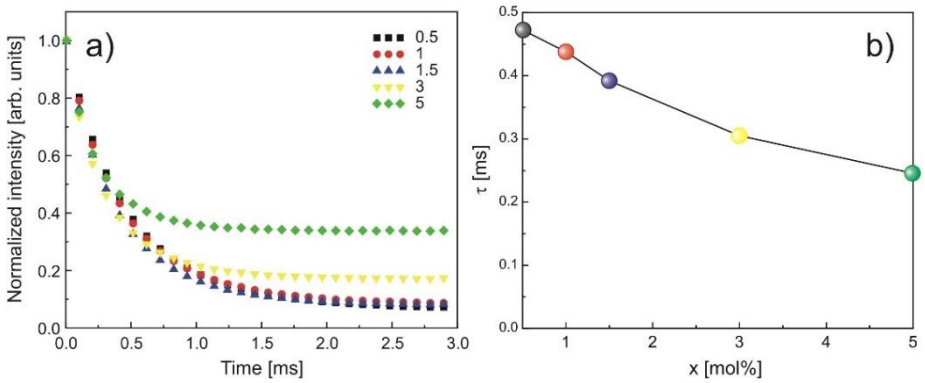

Fig. 5 – a) Lifetimes of the samples with different Eu^{3+} concentrations (from 0.5 to 5 mol%); b) concentration dependence of lifetime values.

3.4. CIE COLOR COORDINATES

To evaluate the color of the synthesized phosphor samples, CIE chromaticity coordinates were derived from the spectra shown in Fig. 4, and other colorimetric values were derived from these data (see Table 2). Figure 6 depicts the variation of CIE coordinates with the excitation wavelength and doping concentration. The color of Y_3NbO_7:*x*Dy^{3+} phosphors can be tuned with different excitation wavelengths, ranging from near-white (Fig. 6a) and 6b) to blue (Fig. 6c) and orange (Fig. 6d).

The dominant wavelength (λ_{dom}) is estimated graphically by extrapolating the straight line starting from the CIE Standard Illuminant E (x_s = 0.333, y_s = 0.333) through the calculated CIE coordinates (x, y) [30]. The color purity (CP) is calculated from [41]:

$$\mathrm{CP} = \sqrt{\frac{(x - x_s)^2 + (y - y_s)^2}{(x_d - x_s)^2 + (y_d - y_s)^2}} \tag{3}$$

where (x_d, y_d) are the coordinates of the dominant wavelength. The value of 100% of CP corresponds to the monochromatic light, while the Standard Illuminant has

a value of 0%. We estimated the correlated color temperature from the equation [42, 43]:

$$\mathrm{CCT} = -449n^3 + 3525n^2 - 6823.3n + 5520.33, \quad (4)$$

that gives the closest matching to the Planckian locus, where $n = (x - 0.3320) / (y - 0.1858)$.

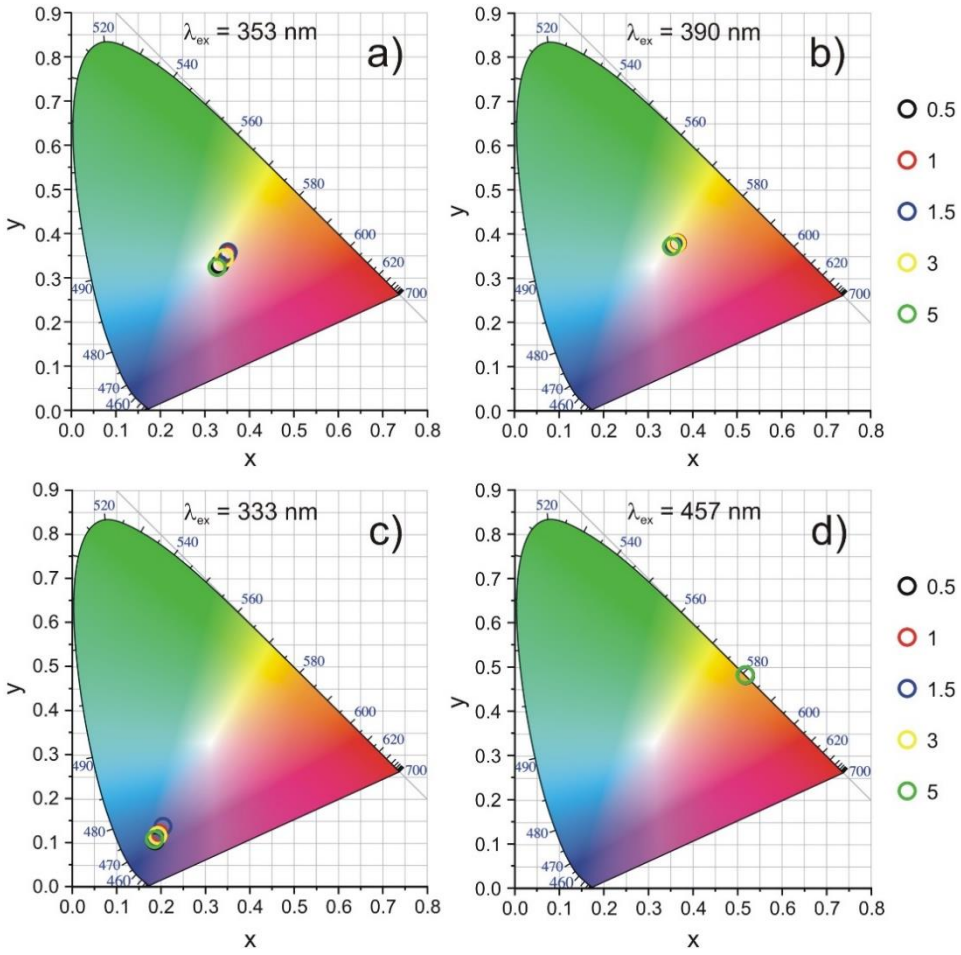

Fig. 6 – CIE chromaticity coordinates of Y_3NbO_7:xDy^{3+} samples (x = 0.5, 1, 1.5, 3, 5 mol%), recorded under: a) λ_{ex} = 353 nm; b) λ_{ex} = 390 nm; c) λ_{ex} = 333 nm, and d) λ_{ex} = 457 nm excitation wavelengths.

When excited with a 333 nm light, the Y_3NbO_7:xDy^{3+} phosphors emit blue color of about 463 nm, and the highest color purity of 76.4% for the sample with 0.5 mol%

of Dy^{3+}. The excitations with 353 and 390 nm lead to the near-white emission of the samples with the corresponding color temperature of ~5000 K and the color purity values close to the one of the Standard Illuminant. The excitation with 353 nm produces white light emission of better quality than under 390 nm irradiation. These results indicate a potential usage of the Dy-doped Y_3NbO_7 phosphors for white LEDs. Compared to the recently reported Dy-doped novel phosphors for WLEDs, our samples' color coordinates and purity are much closer to the Standard Illuminant values [40]. Upon the 457 nm excitation, Y_3NbO_7:*x*Dy^{3+} samples become bright orange phosphors, with a dominant wavelength of 581 nm, color purity of 100% and corresponding color temperature of 2500 K, independent of Dy^{3+} concentration.

Table 2

CIE coordinates (*x*, *y*), corresponding color temperature (CCT), color purity (CP), and dominant wavelength (λ_{dom}) of Y_3NbO_7 samples doped with different Dy^{3+} concentrations and excited with different wavelengths

x [mol%]	λ_{exc} [nm]	*x*	*y*	CCT [K]	λ_{dom} [nm]	CP [%]
0.5	333	0.186194	0.104183	N/A	462.1	76.4
1	333	0.196153	0.120747	N/A	462.4	71
1.5	333	0.204027	0.136749	N/A	463.6	66.2
3	333	0.192326	0.116218	N/A	462.8	72.7
5	333	0.185218	0.107234	N/A	463.3	76
0.5	353	0.332954	0.329294	5471	N/A	N/A
1	353	0.35015	0.353071	4816	576.1	11
1.5	353	0.352035	0.357848	4769	574.8	13
3	353	0.343665	0.34436	5032	577.3	6.4
5	353	0.327326	0.323477	5754	458.1	3.2
0.5	390	0.35298	0.371812	4797	570.2	17.5
1	390	0.365587	0.37924	4440	573.8	23.5
1.5	390	0.357002	0.375635	4684	571.2	19.9
3	390	0.3635	0.378293	4497	573.3	22.6
5	390	0.35298	0.371812	4797	570.2	17.5
0.5	457	0.517449	0.481638	2509	580.8	100
1	457	0.517223	0.481863	2513	580.7	100
1.5	457	0.518227	0.480863	2497	580.9	100
3	457	0.516852	0.482231	2519	580.7	100
5	457	0.517088	0.48195	2515	580.7	100

4. CONCLUSION

Dy^{3+}-doped Y_3NbO_7 phosphor powders with tunable emission color were successfully obtained by a solid-state reaction in a vibrational mill, followed by temperature annealing.

By performing a solid-state reaction, followed by temperature annealing, it was possible to obtain Dy^{3+}-doped Y_3NbO_7 phosphor powders with tunable emission color. XRD analysis reveals that the powders produced are pure-phase with crystallite

sizes in the range of 19 to 60 nm. Changing the excitation wavelength modifies the emission color, from blue (λ_{ex} = 333 nm) and near-white (λ_{ex} = 353 and 390 nm) to orange (λ_{ex} = 457 nm). Samples with Dy^{3+} concentrations greater than 1 mol% have their emission intensity diminished. The emission lifetime values decrease monotonously from 0.472 ms at a concentration of 0.5 mol% Dy^{3+} to 0.246 ms at a concentration of 5 mol% Dy^{3+}. Under 353 nm and 390 nm irradiation, the chromaticity of Y_3NbO_7:xDy^{3+} powders exhibit a correlated color temperature of approximately 4000–5000 K, making them potential near-white phosphors. Excitation at 457 nm produces orange emission with the highest color purity of 100 percent and corresponding color temperature of 2500 K, while excitation at 333 nm produces blue emission. In order to assess further the applicability of these phosphors, we plan to investigate the influence of temperature on color purity, as well as the possible use of these samples as luminescent temperature sensors.

Acknowledgements. The authors acknowledge the financial support of the Ministry of Science, Technological Development and Innovation of the Republic of Serbia, Grant No. 451-03-47/2023-01/200017.

REFERENCES

1. M. Yu, J. Lin, Z. Wang, J. Fu, S. Wang, H.J. Zhang, Y.C. Han, *Fabrication, patterning, and optical properties of nanocrystalline YVO₄:A (A = Eu^{3+}, Dy^{3+}, Sm^{3+}, Er^{3+}) phosphor films via sol-gel soft lithography*, Chem. Mater. **14**(5), 2224–2231 (2002).
2. J.M. Nedelec, D. Avignant, R. Mahiou, *Soft chemistry routes to YPO₄-based phosphors: Dependence of textural and optical properties on synthesis pathways*, Chem. Mater. **14**(2), 651–655 (2002).
3. K. Riwotzki, H. Meyssamy, A. Kornowski, M. Haase, *Liquid-Phase Synthesis of Doped Nanoparticles: Colloids of Luminescing LaPO₄:Eu and CePO₄:Tb Particles with a Narrow Particle Size Distribution*, J. Phys. Chem. B **104**, 2824–2828 (2000).
4. B. Yan, X.-Q. Su, *LuVO₄:RE^{3+} (RE = Sm, Eu, Dy, Er) phosphors by in-situ chemical precipitation construction of hybrid precursors*, Opt. Mater. **29**, 547–551 (2007).
5. E.C. Karsu, E.J. Popovici, A. Ege, M. Morar, E. Indrea, T. Karali, N. Can, *Luminescence study of some yttrium tantalate-based phosphors*, J. Lumin. **131**(5), 1052–1057 (2011).
6. X. Wang, X. Li, H. Yu, S. Xu, J. Sun, L. Cheng, X. Zhang, J. Zhang, Y. Cao, B. Chen, *Effects of Bi^{3+} on down-/up-conversion luminescence, temperature sensing and optical transition properties of Bi^{3+}/Er^{3+} co-doped YNbO₄ phosphors*, J. Rare Earths **40,** 381–389 (2022).
7. S. Yuan, S. Zhao, L. Lou, D. Zhu, Z. Mu, F. Wu, *Fluorescence intensity ratio optical thermometer YNbO₄: Pr^{3+}, Tb^{3+} based on intervalence charge transfer*, Powder Technol. **395**, 83–92 (2022).
8. C. Niu, L. Li, X. Li, Y. Lv, X. Lang, *Upconversion photoluminescence properties of Ho^{3+}/Yb^{3+} co-doped YNbO₄ powder*, Opt. Mat. **75**, 68–73 (2018).
9. F.F. do Carmo, J.P.C. do Nascimento, M.X. Façanha, A.S.B. Sombra, *Warm-white light emission in Er^{3+}/Tm^{3+}/Yb^{3+} tri-doped YNbO₄ phosphor under 808 nm excitation: A synergistic upconversion effect*, Mat. Lett. **254**, 65–68 (2019).
10. Lj.R. Đačanin, S.R. Lukić-Petrović, D.M. Petrović, M.G. Nikolić, M.D. Dramićanin, *Temperature quenching of luminescence emission in Eu^{3+}- and Sm^{3+}-doped YNbO₄ powders*, Journal of Luminescence **151**, 82–87 (2014).
11. Lj.R. Đačanin, M.D. Dramićanin, S.R. Lukić-Petrović, D.M. Petrović, M.G. Nikolić, T.B. Ivetić, I.O. Gúth, *Mechanochemical synthesis of YNbO₄:Eu nanocrystalline powder and its structural, microstructural and photoluminescence properties*, Ceram. Int. **40**, 8281–8286 (2014).

12. Lj. Đačanin Far, S.R. Lukić-Petrović, V. Đorđević, K. Vuković, E. Glais, B. Viana, M.D. Dramićanin, *Luminescence temperature sensing in visible and NIR spectral range using Dy^{3+} and Nd^{3+} doped $YNbO_4$*, Sens. Actuator Phys. **270**, 89–96 (2018).
13. A. Walasek, J. Zhang, S. Wang, E. Zych, *Synthesis and up-converted luminescence of Y_3NbO_7:Er*, Opt. Mat. **30**, 188–191 (2007).
14. K.-Y. Kim, A. Durand, J.-M. Heintz, A. Veillere, V. Jubera, *Spectral evolution of Eu^{3+} doped Y_3NbO_7 niobate induced by temperature*, J. Solid State Chem. **235**, 169–174 (2016).
15. K.-Y. Kim, U.-C. Chung, B. Mutulet, F. Weill, A. Demourgues, J. Rossit, J.-M. Heintz, A. Veillere, V. Jubera, *Tailoring the composition of Eu^{3+}-doped Y_3NbO_7 niobate: structural features and luminescent properties induced by spark plasma sintering*, Inorg. Chem. **56**, 4495–4503 (2017).
16. S. Guene-Girard, J. Courtois, M. Dussauze, J-M. Heintz, A. Fargues, J. Roger, M. Nalin, T. Cardinal, V. Jubera, *Comparison of structural and spectroscopic properties of Ho^{3+}-doped niobate compounds*, Mat. Res. Bull. **143**, 111451 (2021).
17. F.B. Xiong, S.D. Chen, W.B. Yang, X.G. Meng, E. Ma, W. Zhu, *Novel niobates Y_3NbO_7: Ln^{3+} (Ln=Pr, Sm) phosphors for warm white LED: Synthesis and luminescent properties*, Opt. Mat. **128**, 112390 (2022).
18. Lj. Đačanin Far, A. Ćirić, Z. Ristić, J. Periša, T. Dramićanin, S.R. Lukić-Petrović, M.D. Dramićanin, *Photoluminescence of Y_3NbO_7:Eu^{3+} powders*, Ceram. Int. **48**, 28250–28257 (2022).
19. B. Zhang, S. Ying, S. Wang, L. Han, J. Zhang, B. Chen, *Blue-green-yellow color-tunable luminescence of Ce^{3+}-, Tb^{3+}-, and Mn^{2+}-codoped $Sr_3YNa(PO_4)_3F$ via efficient energy transfer*, Inorg. Chem. **58**, 4500–4507 (2019).
20. A. C. Duke, S. Hariyani, J. Brgoch, *$Ba_3Y_2B_6O_{15}$:Ce^{3+} – a high symmetry, narrow-emitting blue phosphor for wide-gamut white lighting*, Chem. Mater. **30**, 2668–2675 (2018).
21. R. Shrivastava, J. Kaur, V. Dubey, *White Light Emission by Dy^{3+} Doped Phosphor Matrices: A Short Review*, J. Fluoresc. **26**, 105–111 (2016).
22. Y. Doi, Y. Harada, Y. Hinatsu, *Crystal structures and magnetic properties of fluorite related oxides Ln_3NbO_7 (Ln=lanthanides)*, J. Solid State Chem. **182**, 709–715 (2009).
23. A.N. Klimenko, Y. Kozlov, V.S. Sergeev, E.A. Pastukhov, *High temperature phase transitions in rare-earth element niobates R_3NbO_7*, Thermochim. Acta **209**, 331–338 (1992).
24. L. Cai, C. Nino, *Structure and dielectric properties of Ln_3NbO_7 (Ln = Nd, Gd, Dy, Er, Yb and Y)*, J. Eur. Ceram. Soc. **27**, 3971–3976 (2007).
25. D. Marrocchelli, P.A. Madden, S.T. Norberg, S. Hull, *Cation composition effects on oxide conductivity in the $Zr_2Y_2O_7$–Y_3NbO_7 system*, J. Phys. Condens. Matter **21,** 405403 (2009).
26. R.D. Shannon, *Revised Effective Ionic Radii and Systematic Studies of Interatomic Distances in Halides and Chalcogenides*, Acta Cryst. A **32**, 751–767 (1976).
27. H.P. Rooksby, E.A.D White, *Rare-earth niobates and tantalates of defect fluorite- and weberite-type structures*, J. Am. Ceram. Soc. **47**, 94–96 (1964).
28. W.T. Carnall, P.R. Fields, K. Rajnak, *Electronic Energy Levels in the Trivalent Lanthanide Aquo Ions. I. Pr^{3+}, Nd^{3+}, Pm^{3+}, Sm^{3+}, Dy^{3+}, Ho^{3+}, Er^{3+} and Tm^{3+}*, J. Chem. Phys. **49**, 4424–4442 (1968).
29. W.T. Carnall, H. Crosswhite, H.M. Crosswhite, *Energy Level Structure and Transition Probabilities in the Spectra of the Trivalent Lanthanides in LaF_3*, Argonne: Lemont, IL, USA, 1978.
30. A. Ćirić, S. Stojadinović, *Photoluminescence of ZrO_2:Gd^{3+} and ZrO_2:Dy^{3+} coatings formed by the plasma electrolytic oxidation*, J. Alloys Compd. **832**, 154907 (2020).
31. M. Gaft, R. Reisfeld, G. Panczer, *Interpretation of Luminescence Centers*, 2015, pp. 221–420
32. G. Blasse, B.C. Grabmaier, *Luminescent Materials*, Springer-Verlag, Berlin, 1994.
33. G. Blasse, A. Bril, *Photoluminescent efficiency of phosphors with electronic transitions in localized centers*, J. Electrochem. Soc. **115**, 1067–1075 (1968).
34. L.H. Brixner, H.Y. Chen, *On the structural and luminescent properties of the M' $LnTaO_4$ rare earth tantalates*, J. Electrochem. Soc. **130**, 2435–2443 (1983).
35. M. Lammers, G. Blasse, *Energy transfer phenomena in Tb^{3+}-activated gadolinium tantalite ($GaTaO_4$)*, Mater. Res. Bull. **19,** 759–768 (1984).

36. B. Yan, X. Xiao, *Novel $YNbO_4:RE^{3+}$ (RE = Sm, Dy, Er) microcrystalline phosphors: Chemical co-precipitation synthesis from hybrid precursor and photoluminescent properties*, Journal of Alloys and Compounds **433**, 251–255 (2007).
37. V. Lojpur, Ž. Antić, M.D. Dramićanin, *Temperature sensing from the emission rise times of Eu^{3+} in SrY_2O_4*, Phys. Chem. Chem. Phys. **16**(46), 25636–25641 (2014).
38. P. Phogat, V.B. Taxak, R.K. Malik, *Crystallographic and optical characteristics of ultraviolet-stimulated Dy^{3+}-Doped $Ba_2GdV_3O_{11}$ Nanorods*, J. Electron. Mater. **51,** 4541–4554 (2022).
39. Z. Min, Q. Zeng, S. Chen, Y. Qin, C. Yao, *Tunable photoluminescence of $LiNbO_3$: RE^{3+} (RE^{3+} = Dy^{3+}, Sm^{3+}, Dy^{3+}/Sm^{3+}) single-phase phosphors for warm white LEDs*, J. Alloy. Compd. **924**, 166497 (2022).
40. B. Deng, J. Jiang, W. Chen, A. Zhang, Z. Liang, F. Li, F. Zeng, G. Zhang, *New Dy^{3+}-activated $KCa_2Nb_3O_{10}$ yellow-emitting phosphors for w-LEDs application: Preparation and optical properties*, Inorg. Chem. Commun. **145**, 110051 (2022).
41. X. Wang, Z. Zhao, Q. Wu, C. Wang, Q. Wang, L. Yanyan, Y. Wang, *Structure, photoluminescence and abnormal thermal quenching behavior of Eu^{2+}-doped $Na_3Sc_2(PO_4)_3$: a novel blue-emitting phosphor for n-UV LEDs*, J. Mater. Chem. C. **4**, 8795–8801 (2016).
42. C.S. McCamy, *Correlated color temperature as an explicit function of chromaticity coordinates*, Color Res. Appl. **17,** 142–144 (1992).
43. J. Hernandez-Andres, R.L. Lee, J. Romero, *Calculating correlated color temperatures across the entire gamut of daylight and skylight chromaticities*, Appl. Optic. **38**, 5703–5709 (1999).